

Towards a Pixel TPC: construction and test of a 32 chip GridPix detector

M. van Beuzekom^a, Y. Bilevych^b, K. Desch^b, S. van Doesburg^a,
H. van der Graaf^a, F. Hartjes^a, J. Kaminski^b, P.M. Kluit^a, N. van der Kolk^a,
C. Ligtenberg^a, G. Raven^a, J. Timmermans^a

^a*Nikhef, Science Park 105, 1098 XG Amsterdam, The Netherlands*

^b*Physikalisches Institut, University of Bonn, Nussallee 12, 53115 Bonn,
Germany*

Abstract

A Time Projection Chamber (TPC) module with 32 GridPix chips was constructed and the performance was measured using data taken in a testbeam at DESY in 2021. The GridPix chips each consist of a Timepix3 chip with integrated amplification grid and have a high efficiency to detect single ionisation electrons. In the testbeam setup, the module was placed in between two sets of Mimosas26 silicon detector planes that provided external high precision tracking and the whole detector setup was slid into the PCMag magnet at DESY. The analysed data were taken at electron beam momenta of 5 and 6 GeV/c and at magnetic fields of 0 and 1 Tesla(T).

The result for the transverse diffusion coefficient D_T is $287 \mu\text{m}/\sqrt{cm}$ at $B = 0$ T and D_T is $121 \mu\text{m}/\sqrt{cm}$ at $B = 1$ T. The longitudinal diffusion coefficient D_L is measured to be $268 \mu\text{m}/\sqrt{cm}$ at $B = 0$ T and $252 \mu\text{m}/\sqrt{cm}$ at $B = 1$ T. Results for the tracking systematical uncertainties in xy (pixel plane) were measured to be smaller than $13 \mu\text{m}$ with and without magnetic field. The tracking systematical uncertainties in z (drift direction) were smaller than $15 \mu\text{m}$ ($B = 0$ T) and $20 \mu\text{m}$ ($B = 1$ T). Finally, the result for the dE/dx resolution for a MIP particle based on a 1 metre track and a realistic GridPix coverage of 60% was measured to be 4% in a 1 T magnetic field.

Keywords: Micromegas, gaseous pixel detector, micro-pattern gaseous

*Corresponding author. Telephone: +31 20 592 2000
Email address: s01@nikhef.nl (P.M. Kluit)
Preprint submitted to Elsevier

30 **1. Introduction**

31 Earlier publications on a single chip [1] and four chip (quad) GridPix detec-
 32 tors [2] showed the potential of the GridPix technology and the large range of
 33 applications for these devices [3]. In particular, it was demonstrated that single
 34 ionisation electrons can be detected with high efficiency and great precision,
 35 allowing excellent 3D track position measurements and particle identification
 36 based on the number of electrons and clusters.

37 As a next step towards a Pixel Time Projection Chamber for a future col-
 38 lider experiment [4], [5], a module consisting of 32 GridPix chips based on the
 39 Timepix3 chip was constructed.

40 A GridPix detector consists of a CMOS pixel Timepix3 chip [6] with inte-
 41 grated amplification grid added by Micro-electromechanical Systems (MEMS)
 42 postprocessing techniques. The Timepix3 chip can be operated with a low
 43 threshold of $515 e^-$, and has a low equivalent noise charge of about $70 e^-$. The
 44 GridPix single chip and quad detectors have a very fine granularity of 55×55
 45 μm and a high efficiency to detect single ionisation electrons.

46 Based on the experience gained with these detectors a 32 GridPix chip mod-
 47 ule - consisting of 8 quads - was built. A drift box defining the electric field
 48 and gas envelop was constructed. A readout system for up to 128 chips with 4
 49 multiplexers readout by one speedy pixel detector readout SPIDR board [7] [8]
 50 was designed. After a series of tests using the laser setup [9] and cosmics in the
 51 laboratory at Nikhef, the detector was taken to DESY for a two week testbeam
 52 campaign.

53 At DESY the 32 chip detector was placed in between two sets of Mimosas26
 54 silicon detector planes and mounted on a movable stage. The whole detector
 55 setup was slid into the centre of the PCMAG magnet at DESY. A beam
 56 trigger was provided by scintillator counters. The data reported here were taken
 57 at different stage positions and electron beam momenta of 5 and 6 GeV/c and

58 at magnetic fields of 0 and 1 T. The performance of the 32 GrixPix chip module
59 was measured using these data sets.

60 **2. The 32 GridPix chip module**

61 A 32 GrixPix chip module was built using the quad module [2] as a basic
62 building block. The quad module consists of four GridPix chips and is optimised
63 for a high fraction of sensitive area of 68.9%. The external dimensions are 39.60
64 x 28.38 mm. The four chips which are mounted on a cooled base plate (COCA),
65 are connected with wire bonds to a common central 6 mm wide PCB. A 10 mm
66 wide guard electrode is placed over the wire bonds 1.1 mm above the aluminium
67 grids, in order to prevent field distortions of the electric drift field. The guard is
68 the main inactive area, and its dimensions are set by the space required for the
69 wire bonds. On the back side of the quad module, the PCB is connected to a
70 low voltage regulator. The aluminium grids of the GridPixes are connected by
71 80 μm insulated copper wires to a high voltage (HV) filtering board. The quad
72 module consumes about 8W of power of which 2W is used in the LV regulator.

73 Eight quad modules were embedded in a box, resulting in a GridPix module
74 with a total of 32 chips. A schematic 3-dimensional drawing of the detector is
75 shown in Figure 1. A schematic drawing of the quads in the module is shown
76 in Figure 2, where also the beam direction is indicated.

77 The internal dimensions of the box are 79 mm along the x -axis, 192 mm along
78 the y -axis, and 53 mm along the z -axis (drift direction), and it has a maximum
79 drift length (distance between cathode and readout anode) of 40 mm. The drift
80 field is shaped by a series of parallel CuBe field wires of 75 μm diameter with
81 a wire pitch of 2 mm and guard strips are located on all of the four sides of the
82 active area. In addition, six guard wires - shown with dashed lines in Figure
83 2 - are suspended over the boundaries of the chips, where no guard is present,
84 to minimise distortions of the electric drift field. The wires are located at a
85 distance of 1.15 mm from the grid planes, and their potential is set to the drift
86 potential at this drift distance. The box has two Kapton 50 μm windows to

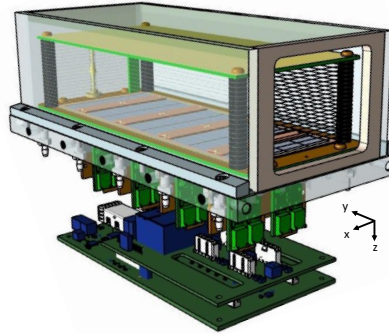


Figure 1: Schematic 3-dimensional render of the 8-quad module detector for illustration purposes.

87 allow the beam to pass with minimal multiple scattering.

88 The gas volume of 780 ml is continuously flushed at a rate of ~ 50 ml/min
 89 (about 4 volumes/hour) with premixed T2K TPC gas. This gas is a mixture
 90 consisting of 95% Ar, 3% CF_4 , and 2% iC_4H_{10} suitable for large TPCs because
 91 of the low transverse diffusion in a magnetic field and the high drift velocity.

92 The data acquisition system of the quad module was adopted to allow for
 93 reading out multiple quads. A multiplexer card was developed that handles
 94 four quads or 16 chips and combines the Timepix3 data into one data stream.
 95 For the 32 GrixPix module two multiplexers are connected to a SPIDR board

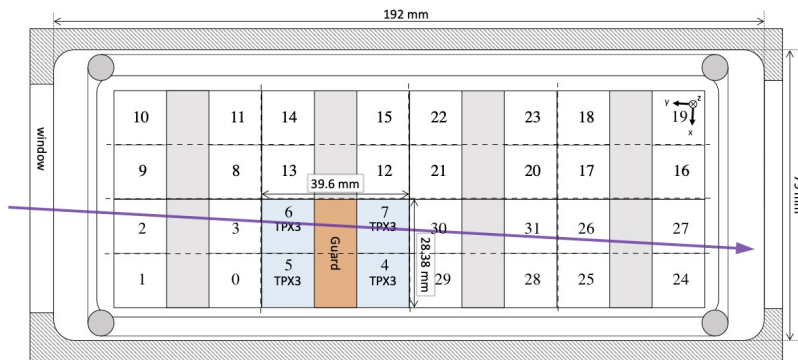


Figure 2: Schematic drawing of the 8-quad module detector with one example quad as viewed from the top of the quads. The chips are numbered and the beam direction is shown in purple.

96 that controls the chips and readout process. The readout speed per chip is 160
97 Mbps and for the multiplexer 2.56 Gbps this corresponds to a maximum rate of
98 21MHits/s. For each pixel the precise Time of Arrival (ToA) using a 640 MHz
99 TDC and the time over threshold (ToT) are measured.

100 **3. Experimental setup**

101 In preparation of the two weeks DESY testbeam campaign, a support frame
102 was designed to move the 32 chip GridPix module in the plane perpendicular to
103 the beam by a remotely controlled stage such that the whole detector volume
104 could be probed. The module was mounted upside down with respect to figure
105 1 to allow access to the electronics from above. The support frame also held
106 three Mimosas26 silicon detector planes [10] - with an active area of (21.2 mm x
107 10.6 mm) - placed in front of the detector and three Mimosas26 planes behind
108 the detector. At DESY the (Mimosas26) silicon detector planes were provided
109 by the testbeam coordinators. The whole detector setup was slid towards
110 the centre of the PCMAG magnet at the DESY II testbeam facility [10]. A
111 beam trigger was provided by a double scintillator counter coincidence. The
112 data were taken at different stage positions to cover the whole sensitive TPC
113 volume. Runs with electron beam momenta of 5 and 6 GeV/c and at magnetic
114 fields of 0 and 1 T were analysed.

115 A photograph of the detector setup in the PCMAG magnet is shown in
116 Figure 3.

117 The experimental and environmental parameters such as temperature, pres-
118 sure, gas flow, oxygen content were measured and logged by a Windows op-
119 erated slow control system. The experimental parameters are summarised in
120 Table 1. The chips were cooled by circulating Glycol through the cooling chan-
121 nels in the module carrier plate. The cooling blocks of the multiplexers were
122 further cooled by blowing pressurised air on them.

123 The data was produced in four main data streams: one stream produced by
124 the Mimosas26 Telescope, two data streams by the two Timepix multiplexers and

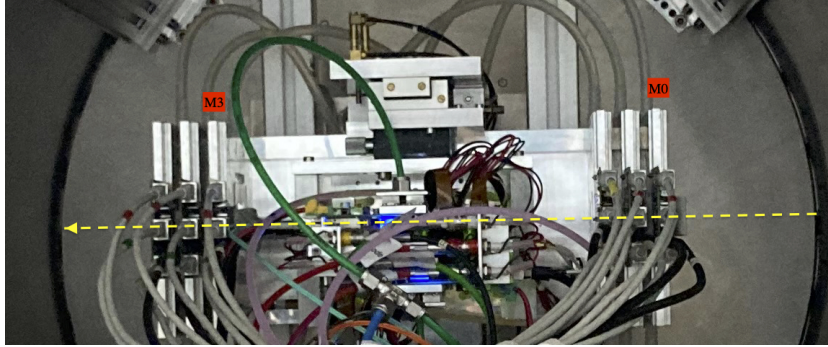


Figure 3: Photo of the detector setup at the centre of the PCMAG magnet. The Mimosa26 planes M0 and M3 are indicated in red as well as the beam direction (yellow). Centrally, the stager positions the TPC module with respect to the beam and the Mimosa26 planes.

Table 1: Overview of the experimental parameters. The ranges indicate the variation over the data taking period

Number of analysed runs at B=0 (1) T	6 (8)
Run duration	10-90 minutes
Number of triggers per run	3-100 k
E_{drift}	280 V/cm
V_{grid}	340V
Threshold	550 e ⁻
Gas temperature	303.3-306.6 K
Pressure	1011 – 1023 mbar
Oxygen concentration	240 - 620 ppm
Water vapour concentration	2000 - 7000 ppm

125 one trigger stream. The double scintillator coincidence provided a trigger signal
126 to the Trigger Logic Unit (TLU) [11] that sends a signal to the telescope readout
127 and the trigger SPIDR. The data acquisition system of the Telescope and trigger
128 SPIDR injected a time stamp into their respective data streams. Hits from the
129 Mimosas26 planes were collected with a sliding window of $-115 \mu\text{s}$ to $230 \mu\text{s}$ of
130 the trigger. The data acquisition of the multiplexer and the trigger SPIDR were
131 synchronised at the start of the run. By comparing the time stamps in these
132 streams, Telescope tracks and TPC tracks could be matched. Unfortunately,
133 the SPIDR trigger had - due to a cabling mistake at the output of the TLU - a
134 common 25nsec time jitter.

135 After a short data taking period one of the chips (nr 11) developed a short
136 circuit and the HV on the grid of the chip was disconnected. After the testbeam
137 data taking period the module was repaired in the clean room in Bonn.

138 4. Analysis

139 4.1. Telescope Track reconstruction procedure

140 The data of the Telescope is decoded and analysed using the Corryvreckan
141 software package [12]. The track model used for fitting was the General Broken
142 Lines (GBL) software [14]. The code was extended and optimised to fit curved
143 broken lines for the data with magnetic field. The telescope planes were itera-
144 tively aligned using the standard alignment software provided by the package.
145 The single point Mimosas26 resolution is $4 \mu\text{m}$ in x and $6 \mu\text{m}$ in z (drift direction)
146 [10].

147 Telescope tracks were selected with at least 5 out of the 6 planes on the track
148 and a total χ^2 of better than 25 per degree of freedom. The uncertainties on the
149 Telescope track prediction in the middle of the GridPix module are dominated
150 by multiple scattering. The amount of multiple scattering was estimated by
151 comparing the predictions from the two telescope arms for $6 \text{ GeV}/c$ tracks at B
152 $= 0 \text{ T}$. The expected uncertainty in x and z is $26 \mu\text{m}$ on average.

153 *4.2. TPC Track reconstruction procedure*

154 GridPx hits are selected requiring a minimum time over threshold ToT of
155 $0.15 \mu\text{s}$. The drift time is defined as the measured time of arrival minus the
156 trigger time recorded in the trigger SPIDR data stream minus a fixed t_0 (the
157 drift time at zero drift). The drift time was corrected for time walk [2] using
158 the measured time over threshold (ToT in units of μs) and the formula (1):

$$\delta t = \frac{18.6(ns\mu s)}{\text{ToT} + 0.1577(\mu s)}. \quad (1)$$

159 Furthermore, small time shift corrections - with an odd-even and a 16x2 pixels
160 structure - coming from the TPX3 clock distribution were extracted from the
161 data and applied.

162 The z drift coordinate was calculated as the product of the drift time and the
163 drift velocity. This implies that $z_{\text{drift}} = -z$ as defined in figure 1. GridPix hits
164 outside an acceptance window of 30 mm wide in x and 15 mm wide in z were
165 not used in the track finding and reconstruction. Based on a Hough transform
166 an estimate of the TPC track position and angles in the middle of the module
167 (at $y = 1436$ pixels) was obtained. This estimate was used to collect the hits
168 around the TPC track and fit the track parameters. For this fit a straight line
169 ($B = 0$ T) or a quadratic track $B = 1$ T model was used. In the fit, the expected
170 uncertainties per hit σ_x and σ_z were used. The fit was iterated three times to
171 perform outlier removal at respectively 10, 5 and 2.5 sigma level. A TPC track
172 was required to have a least 100 hits in each multiplexer. At least 25% of the
173 total number of hits should be on track and the χ^2 per degree of freedom had
174 to be less than 3 in xy and zy. All track parameters were expressed at a plane
175 in the middle of the TPC.

176 The calibration and alignment of the detector was done using high quality
177 tracks for which the track selections are summarised in table 2.

178 The drift velocity was calibrated per run by fitting a linear function to the z
179 (predicted from the Telescope track at the measured TPC hit position) versus
180 the measured drift time in the TPC. For the $B = 0$ T runs it varies between

Table 2: Table with track/event selection cuts

Track/Event Selection
$ x_{\text{TPC}} - x_{\text{Telescope}} < 0.3 \text{ mm}$
$ z_{\text{TPC}} - z_{\text{Telescope}} < 2 \text{ mm}$
$ dx/dy_{\text{TPC}} - dx/dy_{\text{Telescope}} < 4 \text{ mrad}$
$ dz/dy_{\text{TPC}} - dz/dy_{\text{Telescope}} < 2 \text{ mrad}$

181 61.6 and 63.0 $\mu\text{m}/\text{ns}$. For the $B = 1 \text{ T}$ runs it is between 57.2 and 59.1 $\mu\text{m}/\text{ns}$.
 182 The variation comes mainly from the changes in the relative humidity of the
 183 gas volume due to small leaks.

184 The individual TPX3 chips were iteratively aligned fitting a shift in x (z drift)
 185 and two slopes $dx(z \text{ drift})/d \text{ row}(\text{column})$. The alignment was done per run,
 186 because the detector was moved in x and/or z for each run. The fitted slopes
 187 were also corrected for small shifts and rotations (3D) in the nominal chip
 188 position.

189 An example event run 6913 without B field with a TPC and a telescope
 190 track is shown in figure 4. The TPC is located between $y = 0$ and 2872 pixels.
 191 Three Mimosa26 planes are located at $y < -1000$ and three at $y > 4000$ pixels.

192 5. Hit resolutions

193 In order to study the single electron resolution for the data with and without
 194 magnetic field, additional selections on the Telescope and TPC tracks were
 195 applied. Due to the trigger time jitter of 25 nsec (corresponding to 1.5 mm
 196 drift), the prediction of the telescope track in z must be used as the reference for
 197 z . Secondly, the z hits of the TPC track were fitted to correct for the common
 198 time shift and the z residuals were calculated with respect to the fitted TPC
 199 track. In the xy plane the residuals of TPC hits with respect to the telescope
 200 track were used to extract the single electron resolution in xy . For the resolution
 201 studies runs at three different z stage positions of the TPC were selected where

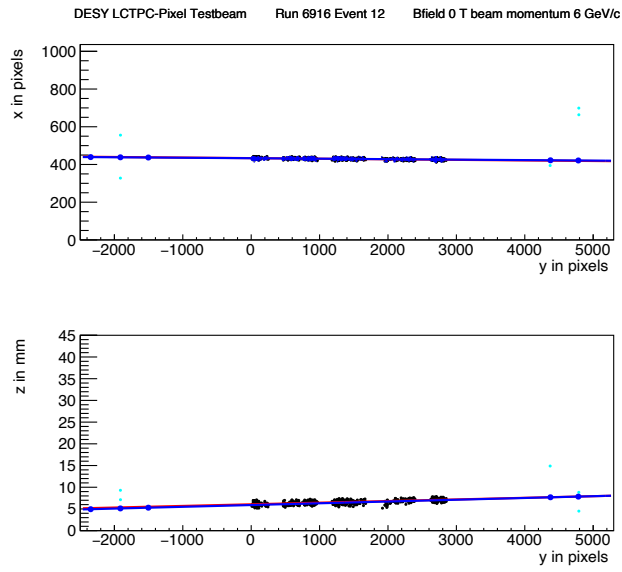


Figure 4: An event display for run 6913 without B field, with in total 1293 TPC hits (black dots) in the precision plane (x,y) and driftplane (z drift,y). The fitted TPC track (red line) with 1130 hits on track and the telescope track (blue line) with 5 Mimosa26 planes (blue hits) on track are shown. In green the off track Mimosa26 hits are shown.

202 the beam gave hits in the central chips. The data of 14 central chips (9, 12, 21,
 203 20, 17, 16, 2, 3, 6, 7, 30, 31, 26 and 27) was used. Two chips (8 and 13) were
 204 left out because of the E field deformations caused by the short circuit in chip
 205 11.

206 5.1. Hit resolutions in the pixel plane

207 The resolution of the hits in the pixel plane (xy) was measured as a function
 208 of the predicted drift position (z_{drift}). Only hits are used crossing the fiducial
 209 region defined by the central core of the beam and staying 20 pixels away from
 210 the chip edges. The resolution for the detection of ionisation electrons σ_x is
 211 given by:

$$\sigma_x^2 = \frac{d_{\text{pixel}}^2}{12} + d_{\text{track}}^2 + D_T^2(z_{\text{drift}} - z_0), \quad (2)$$

212 where d_{pixel} is the pixel pitch size, d_{track} the uncertainty from the track predic-
 213 tion, z_0 is the position of the grid, and D_T is the transverse diffusion coefficient.
 214 The resolution at zero drift distance $d_{\text{pixel}}/\sqrt{12}$ was fixed to 15.9 μm and d_{track}
 215 to 30 μm for $B = 0$ T and 42 μm for $B = 1$ T data. The uncertainty of the track
 216 prediction was measured and is larger than the Mimosa plane resolution because
 217 of multiple scattering in the sensor and in the entrance and exit windows.

218 The expression (2) - leaving z_0 and D_T as free parameters - is fitted to the B
 219 = 0 T data shown in Figure 5. The fit gives a transverse diffusion coefficient D_T
 220 of 287 $\mu\text{m}/\sqrt{cm}$ with negligible statistical uncertainty. The measured value is in
 221 agreement with the value of 287 $\mu\text{m}/\sqrt{cm} \pm 4\%$ predicted by the gas simulation
 222 software Magboltz [15]. The values of the diffusion coefficients depend on the
 223 humidity that was not precisely measured during the testbeam. The humidity
 224 strongly affects the drift velocity. Therefore the drift velocity prediction from
 225 Magboltz was used to determine the water content per run and predictions for
 226 the diffusion coefficients could be obtained.

227 A fit to the $B = 1$ T data, also shown in Figure 5, gives a transverse diffu-
 228 sion coefficient D_T of 121 $\mu\text{m}/\sqrt{cm}$ with negligible statistical uncertainty. The
 229 measured value is in agreement with the value of 119 $\mu\text{m}/\sqrt{cm} \pm 2\%$ predicted
 230 by Magboltz.

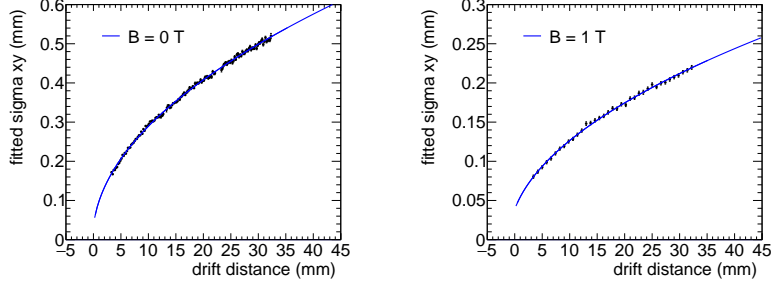


Figure 5: Measured hit resolution in the pixel plane (black points) fitted with the resolution function according to equation (2) (blue line).

231 5.2. Hit resolution in the drift plane

232 The resolution for the detection of ionisation electrons σ_z in the drift plane
 233 is given by:

$$\sigma_z^2 = \sigma_{z0}^2 + d_{\text{track}}^2 + D_L^2(z_{\text{drift}} - z_0), \quad (3)$$

234 where σ_{z0} is the resolution at zero drift distance, d_{track} the expected track
 235 uncertainty and D_L the longitudinal diffusion constant. Only tracks crossing
 236 the fiducial region were accepted and hits with a ToT value above $0.6 \mu\text{s}$ were
 237 selected. Because of the time jitter, the fitted TPC track is used for the drift
 238 residuals. For z_{drift} the Telescope prediction at the hit was used. The expected
 239 uncertainty on the Telescope track prediction is $25 \mu\text{m}$.

240 The expression (3) - leaving σ_{z0} and D_L as free parameters - is fitted to
 241 the $B = 0 \text{ T}$ data shown in Figure 6. The value of z_0 was fixed to the result
 242 of the fit in the xy plane. The value of σ_{z0} was measured to be $138 \mu\text{m}$. The
 243 longitudinal diffusion coefficient D_L was determined to be $(265 \pm 1) \mu\text{m}/\sqrt{\text{cm}}$,
 244 which is higher than the expected value $(236 \pm 3) \mu\text{m}/\sqrt{\text{cm}}$ from a Magboltz
 245 calculation [15].

246 A fit to the $B = 1 \text{ T}$ data shown in Figure 6 gives a longitudinal diffusion
 247 coefficient D_L of $(250 \pm 2) \mu\text{m}/\sqrt{\text{cm}}$. The measured value is in agreement with
 248 the value of $(245 \pm 4) \mu\text{m}/\sqrt{\text{cm}}$ predicted by Magboltz. The fitted value of σ_{z0}
 249 was $133 \mu\text{m}$.

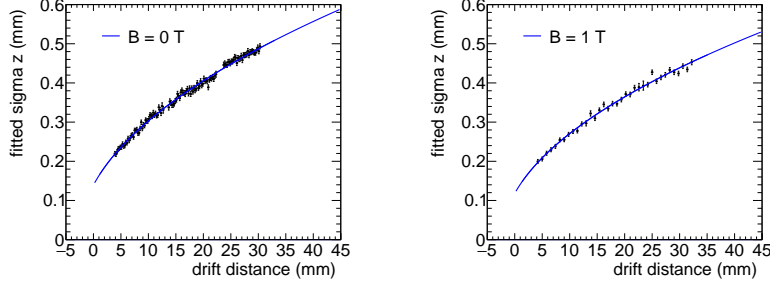


Figure 6: Resolution in the drift plane for hits with a ToT above $0.60 \mu\text{s}$. The data are fitted with the expression of equation (3).

250 5.3. Deformations in the pixel and drift plane

251 It is important to measure possible deformations in the pixel (xy) and drift
 252 (z) plane to quantify the tracking precision. For the construction of a large Pixel
 253 TPC, deformations in the pixel plane deformation should be controlled to better
 254 than typically $20 \mu\text{m}$ because these affect the momentum resolution. The mean
 255 residuals in the pixel and drift planes are shown in Figure 7 for the $B = 0 \text{ T}$
 256 data set using a large set of runs to cover the whole module. The residuals were
 257 calculated with respect to the Telescope track prediction. Because of limited
 258 statistics bins were grouped into 8×16 pixels. Bins with less than 100 hits are
 259 left out and residuals larger (smaller) than $+(-)100 \mu\text{m}$ are shown in red (blue).

260 A few critical areas can be observed in figure 7: the region around chip 11
 261 is affected (chips 14, 8 and 13), because the grid of chip 11 was disconnected.
 262 Deformations are present at the four corners of the drift box (chips 1, 10, 19 and
 263 24) and close to the upper corner edge (chip 16) of the drift box. These come
 264 from inhomogenities in the drift field near the supporting pilars, the field wires
 265 are too close to the chip to provide a constant electric field. It was concluded
 266 that for the deformation results the hits of these nine chips have to be removed.
 267 The track fit was redone leaving these hits out of the fit, such that they could
 268 not bias and affect the results.

269 In order to reduce the statistical fluctuations and quantify the tracking pre-

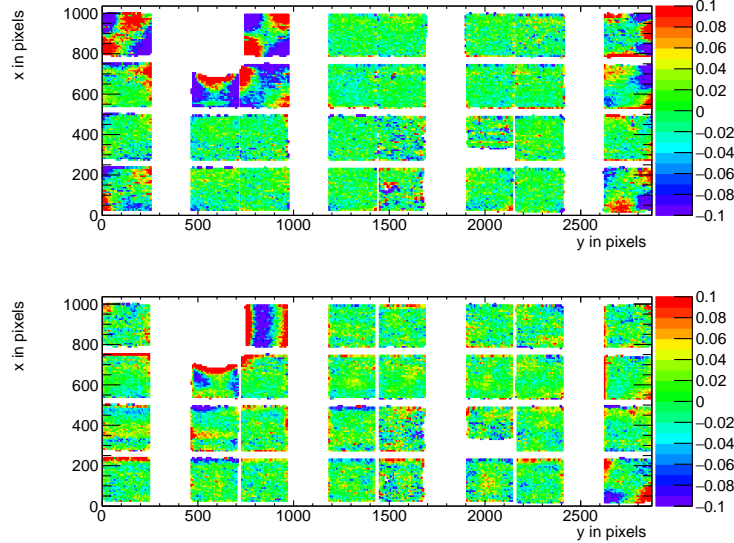


Figure 7: Mean residuals (in mm) in the pixel (top) and drift (bottom) plane for $B = 0$ T data at the expected hit position.

270 cision, the module was regrouped in four 256x256 pixel planes put side by side
 271 on the horizontal axis, as shown in figure 8. Bins have a size of 16x16 pixels and
 272 bins with less than 1000 entries are not shown. A bias in the mean residual at
 273 the edge of the chips is expected to be present for an ideal detector because of
 274 the finite coverage and the diffusion in the drift process. Due to the presence of
 275 the dike pixels at the edge of the chip became covered and inefficient. Therefore
 276 the region near the edge of 5 pixels was removed. For the drift coordinate a
 277 region of 10 pixels was removed. The total number of measurements (bins) in
 278 xy is 895 and in z 892. One can observe that in the module plane no clear sys-
 279 tematic deviations are present and conclude that the guard wire voltages were
 280 on average well tuned. Note that in the quad module we had no guard wires
 281 and deformation corrections had to be applied [2]. The r.m.s. of the distribu-
 282 tion of the measured mean residual over the surface in the pixel plane is $11 \mu\text{m}$
 283 and in the drift plane $15 \mu\text{m}$. Similarly, regrouping the module in four planes
 284 of 256x256 pixels putting them on top of each other vertically, yielded a r.m.s.

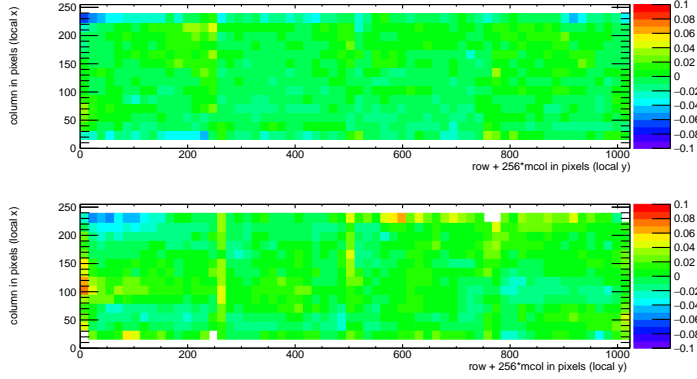


Figure 8: Mean residuals (in mm) in the pixel (top) and drift plane (bottom) for $B = 0$ T data at the regrouped expected hit position.

285 in the pixel plane of $13 \mu\text{m}$ and $13 \mu\text{m}$ in the drift coordinate. The expected
 286 statistical error in xy is $4 \mu\text{m}$ and in z $5 \mu\text{m}$.

287 In the $B = 1$ T data set, the electrons will drift mainly along the magnetic
 288 field lines. Deformations are in that case due to e.g. the non-alignment of the
 289 electric and magnetic field, giving ExB effects. Unfortunately, the statistics of
 290 the Telescope tracks that have a matched TPC track was insufficient and did
 291 not cover the full TPC module plane. Therefore the larger statistics of matched
 292 and unmatched TPC tracks was used. TPC tracks were required to pass angular
 293 selection cuts (dx/dy between -40 and -20 mrad and dz/dy between 0 and 14
 294 mrad) and a momentum cut ($p > 2 \text{ GeV}/c$ and $q < 0$).

295 The mean residuals in the pixel and drift planes are shown in figure 9 for
 296 the $B = 1$ T data set using a large set of runs to cover the whole module. The
 297 residuals were calculated with respect to the TPC track prediction. Because of
 298 limited statistics bins were grouped into 8×16 pixels. Bins with less than 100
 299 hits are left out and residuals larger (smaller) than $+(-)100 \mu\text{m}$ are shown in
 300 red (blue).

301 In figure 9 the critical areas discussed above - around chip 11, the four corner
 302 chips and chip 16 in the upper corner edge - can be clearly observed. For the
 303 deformation results the hits of these nine chips have to be removed. The TPC

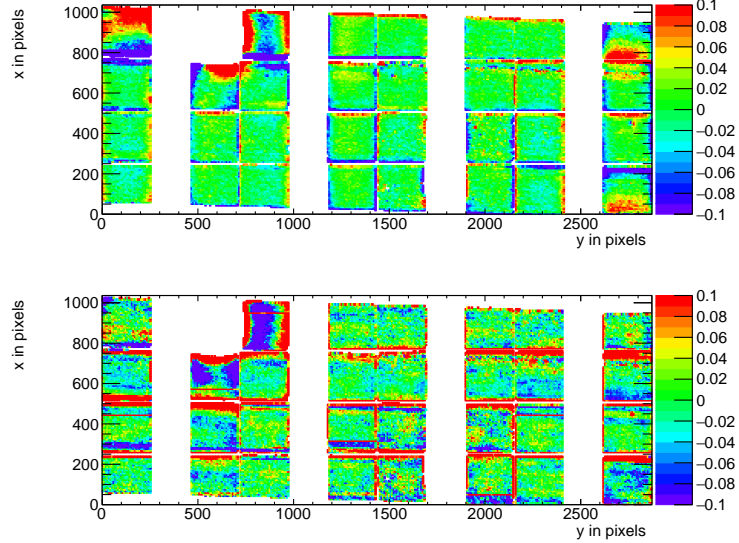


Figure 9: Mean residuals in the pixel and drift plane for $B = 1$ T data at the expected hit position.

304 track fit was redone leaving these hits out of the fit, thus that they could
 305 not bias and affect the results. The TPC plane is well covered, although one
 306 can observe that due to the angle of the beam in the xy plane the chips in the
 307 upper right and lower left corners are not fully covered.

308 In order to reduce the statistical fluctuations and quantify the tracking pre-
 309 cision, the module was regrouped in four 256x256 pixel planes put side by side
 310 on the horizontal axis, as shown in figure 10. Bins have a size of 16x16 pix-
 311 els and bins with less than 1000 entries are not shown. Similar to the no-field
 312 deformations studies, acceptance cuts had to be applied. The region near the
 313 edge of 16 pixels (columns) was removed. For the drift coordinate in addition
 314 a region of 10 pixels (rows) was removed. The total number of measurements
 315 (bins) in xy is 896 and in z 896. One can observe that in the module plane no
 316 clear systematic deviations are present. The r.m.s. of the distribution of the
 317 measured mean residual over the surface in the pixel plane is $13 \mu\text{m}$ and in the
 318 drift plane $19 \mu\text{m}$. Similarly, regrouping the module in four planes of 256x256

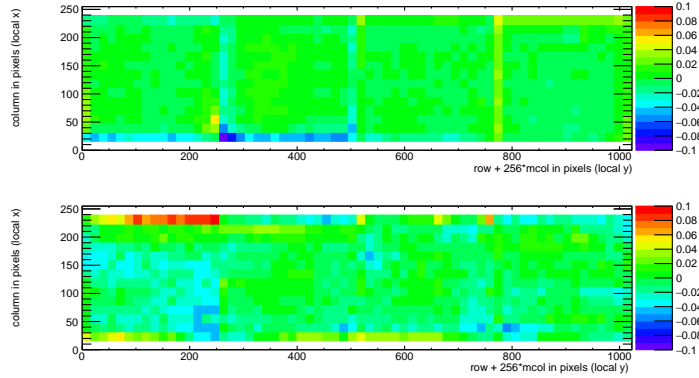


Figure 10: Mean residuals in the pixel and drift plane for B= 1T data at the regrouped expected hit position.

319 pixels side by side vertically, yielded a r.m.s. in the pixel plane of $11 \mu\text{m}$ and
 320 $20 \mu\text{m}$ in the drift coordinate. The expected statistical error in xy is $2 \mu\text{m}$ and
 321 in z $3 \mu\text{m}$.

322 5.4. Tracking resolution

323 A selected TPC track in the B = 0 T data has on average 1000 hits. The
 324 tracking precision in the middle of the TPC was derived on a track-by-track basis
 325 and found to be on average $9 \mu\text{m}$ in the precision plane and $13 \mu\text{m}$ in z. The
 326 angular resolution in dx/dy was on average 0.19 mrad and for dz/dy 0.25 mrad.
 327 It is clear that the position resolution in the TPC in the precision and drift
 328 coordinates is impressive for a track length of (only) 158 mm. The values are
 329 smaller than the uncertainty on the track prediction from the silicon telescope
 330 of $26 \mu\text{m}$ on average that is dominated by multiple scattering.

331 6. Particle Identification using dE/dx

332 The distribution of the number of TPC track hits per chip - without requiring
 333 a matched Telescope track - are shown in figure 11 for the data without magnetic
 334 field and for the B = 1 T data. The B = 0 T data analysis selects the central

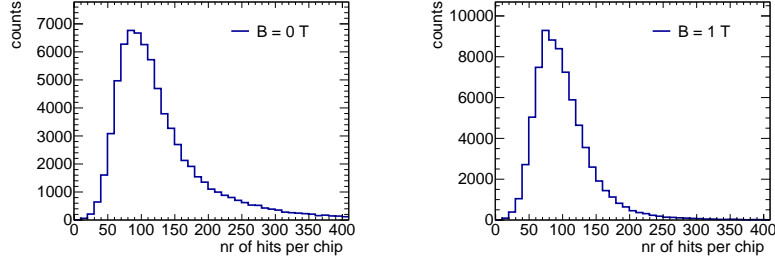


Figure 11: Distribution of the number of track hits per per chip for B = 0 T (left) B = 1 T data.

335 chips 2,6,7,9,16,17,26 and 27. The B = 1 T data analysis selects the same chips
 336 plus chips 12,13,20 and 21.

337 The mean number of hits is measured to be 124 and 89 in the B = 0 T and
 338 1 T data sets respectively. The most probable values are respectively 87 and
 339 64. Note that the B = 0 T data have a much larger Landau-like tail than the
 340 1 T data. Also the fluctuations in the core of the distribution are larger. The
 341 mean time over threshold is $0.68 \mu\text{s}$ for the B = 0 T and $0.86 \mu\text{s}$ at a B = 1
 342 T data. This means that the deposited charge per pixel is smaller for the 0 T
 343 data. The most probable value for the total deposited charge is similar for both
 344 data sets. The mean number of hits is in agreement with the predictions of [13]
 345 106 electron-ion pairs for a $6 \text{ GeV}/c$ electron at B = 0 T, crossing 236 pixels or
 346 12.98 mm and a detector running at 85% single electron efficiency.

347 7. Conclusion and outlook

348 A Time Projection Chamber module with 32 GridPix chips was constructed
 349 and the performance was measured using data taken in a testbeam at DESY
 350 in 2021. The analysed data were taken at electron beam momenta of 5 and 6
 351 GeV/c and at magnetic fields of 0 and 1 T.

352 The result for the transverse diffusion coefficient D_T is $287 \mu\text{m}/\sqrt{cm}$ at B =
 353 0 T and D_T is $121 \mu\text{m}/\sqrt{cm}$ at B = 1 T. The longitudinal diffusion coefficient
 354 D_L is measured to be $268 \mu\text{m}/\sqrt{cm}$ at B = 0 T and $252 \mu\text{m}/\sqrt{cm}$ at B = 1 T.

355 Results for the tracking systematical uncertainties in xy were measured to be
356 smaller than $13\ \mu\text{m}$ with and without magnetic field. The tracking systematical
357 uncertainties in z were smaller than $15\ \mu\text{m}$ ($B = 0\ \text{T}$) and $20\ \mu\text{m}$ ($B = 1\ \text{T}$).

358 Not all data were analysed and users are welcome to study them using the
359 data sets on available on the Grid.

360 The GridPix detector will be further tested and developed in view of a TPC
361 that will be installed in a heavy ion experiment at the EIC.

362 **Acknowledgements**

363 This research was funded by the Netherlands Organisation for Scientific Re-
364 search NWO. The authors want to thank the support of the mechanical and
365 electronics departments at Nikhef and the detector laboratory in Bonn. The
366 measurements leading to these results have been performed at the Test Beam
367 Facility at DESY Hamburg (Germany), a member of the Helmholtz Association
368 (HGF).

369 **References**

- 370 [1] C. Ligtenberg, et al., Performance of a GridPix detector based on the
371 Timepix3 chip, Nucl. Instrum. Meth. A 908 (2018) 18–23. [arXiv:1808.04565](#), [doi:10.1016/j.nima.2018.08.012](#).
- 372
- 373 [2] C. Ligtenberg, et al., Performance of the GridPix detector quad, Nucl.
374 Instrum. Meth. A 956 (2020) 163331. [arXiv:2001.01540](#), [doi:10.1016/j.nima.2019.163331](#).
- 375
- 376 [3] J. Kaminski, Y. Bilevych, K. Desch, C. Krieger, M. Lupberger, GridPix de-
377 tectors - introduction and applications, Nucl. Instrum. Meth. A845 (2017)
378 233–235. [doi:10.1016/j.nima.2016.05.134](#).
- 379 [4] C. Ligtenberg, A GridPix TPC readout for the ILD experiment at the
380 future International Linear Collider, Ph.D. thesis, Free University of

- 381 Amsterdam (2021).
382 URL [https://www.nikhef.nl/pub/services/biblio/theses_pdf/](https://www.nikhef.nl/pub/services/biblio/theses_pdf/thesis_C_Ligtenberg.pdf)
383 [thesis_C_Ligtenberg.pdf](https://www.nikhef.nl/pub/services/biblio/theses_pdf/thesis_C_Ligtenberg.pdf)
- 384 [5] M. Lupberger, Y. Bilevych, H. Blank, D. Danilov, K. Desch, A. Hamann,
385 J. Kaminski, W. Ockenfels, J. Tomtschak, S. Zigann-Wack, Toward the
386 Pixel-TPC: Construction and Operation of a Large Area GridPix Detector,
387 IEEE Trans. Nucl. Sci. 64 (5) (2017) 1159–1167. doi:10.1109/TNS.2017.
388 2689244.
- 389 [6] T. Poikela, J. Plosila, T. Westerlund, M. Campbell, M. De Gaspari,
390 X. Llopart, V. Gromov, R. Kluit, M. van Beuzekom, F. Zappone,
391 V. Zivkovic, C. Brezina, K. Desch, Y. Fu, A. Kruth, Timepix3: a 65K
392 channel hybrid pixel readout chip with simultaneous ToA/ToT and sparse
393 readout, JINST 9 (05) (2014) C05013.
394 URL <http://stacks.iop.org/1748-0221/9/i=05/a=C05013>
- 395 [7] J. Visser, M. van Beuzekom, H. Boterenbrood, B. van der Heijden, J. I.
396 Muñoz, S. Kulis, B. Munneke, F. Schreuder, SPIDR: a read-out system for
397 Medipix3 & Timepix3, Journal of Instrumentation 10 (12) (2015) C12028.
398 doi:10.1088/1748-0221/10/12/C12028.
- 399 [8] B. van der Heijden, J. Visser, M. van Beuzekom, H. Boterenbrood, S. Kulis,
400 B. Munneke, F. Schreuder, SPIDR, a general-purpose readout system for
401 pixel ASICs, JINST 12 (02) (2017) C02040. doi:10.1088/1748-0221/12/
402 02/C02040.
- 403 [9] F. Hartjes, A diffraction limited nitrogen laser for detector calibration in
404 high energy physics, Ph.D. thesis, University of Amsterdam (1990).
405 URL [https://www.nikhef.nl/pub/services/biblio/theses_pdf/](https://www.nikhef.nl/pub/services/biblio/theses_pdf/thesis_F_Hartjes.pdf)
406 [thesis_F_Hartjes.pdf](https://www.nikhef.nl/pub/services/biblio/theses_pdf/thesis_F_Hartjes.pdf)
- 407 [10] R. Diener et al., The DESY II test beam facility, Nuclear Instruments
408 and Methods in Physics Research. Section A: Accelerators, Spectrometers,

- 409 Detectors and Associated Equipment 922 (2019) 265–286. `arXiv:1807.`
410 `09328`, `doi:10.1016/j.nima.2018.11.133`.
- 411 [11] P. Baesso, D. Cussans, J. Goldstein, The AIDA-2020 TLU: a flexible trigger
412 logic unit for test beam facilities, *Journal of Instrumentation* 14 (09) (2019)
413 P09019–P09019. `arXiv:2005.00310`.
414 URL `https://doi.org/10.1088/1748-0221/14/09/p09019`
- 415 [12] D. Dannheim, K. Dort, L. Huth, D. Hynds, I. Kremastiotis, J. Kröger,
416 M. Munker, F. Pitters, P. Schütze, S. Spannagel, T. Vanat, M. Williams,
417 Corryvreckan: a modular 4d track reconstruction and analysis software
418 for test beam data, *Journal of Instrumentation* 16 (03) (2021) P03008.
419 `doi:10.1088/1748-0221/16/03/p03008`. `arXiv:2011.12730`.
420 URL `https://doi.org/10.1088/1748-0221/16/03/p03008`
- 421 [13] R. Veenhof, Garfield - simulation of gaseous detectors, version 9, Reference
422 W5050 (1984-2010).
423 URL `https://garfield.web.cern.ch`
- 424 [14] C. Kleinwort, General broken lines as advanced track fitting method, *Nu-*
425 *clear Instruments and Methods in Physics Research Section A: Acceler-*
426 *ators, Spectrometers, Detectors and Associated Equipment* 673 (2012) 107–
427 110. `doi:10.1016/j.nima.2012.01.024`.
- 428 [15] S. F. Biagi, Monte Carlo simulation of electron drift and diffusion in count-
429 ing gases under the influence of electric and magnetic fields, *Nucl. Instrum.*
430 *Meth. A*421 (1-2) (1999) 234–240. `doi:10.1016/S0168-9002(98)01233-9`.
431 URL `https://magboltz.web.cern.ch/magboltz`